26 HIGH-SPEED PHOTODETECTORS

John E. Bowers and Yih G. Wey

Department of Electrical and Computer Engineering
University of California
Santa Barbara, California

26.1 GLOSSARY

A	area
A^{**}	modified effective Richardson constant
$A_e(A_h)$	electron (hole) ionization parameters
B	bit rate
C_J	junction capacitance
C_P	pad capacitance
$D_e(D_h)$	diffusion coefficient for electrons (holes)
$\mathbf{E}$	electric field
$e_n(e_p)$	emission functions for electrons (holes)
F	frequency response
f	frequency
$f_{3\text{dB}}$	3-dB bandwidth
G	photoconductor gain
H	transfer function
h	Plank's constant
I_d	dark current
I_{dm}	multiplied dark current
I_{du}	unmultiplied dark current
I_{ph}	photocurrent
i	current
$\langle i_{\text{na}}^2 \rangle$	amplifier noise power
J	current density
J_{DIFF}	diffusion component of current density
J_{DRIFT}	drift component of current density

$J_e(J_h)$	electron (hole) component of current density
k	ratio of electron to hole ionization coefficient
k_b	Boltzmann constant
L	absorption layer thickness
$L_e(L_h)$	diffusion length for electrons (holes)
L_s	series inductance
M	multiplication factor
$M_n(M_p)$	electron (hole) initiated multiplication factor
m	electron mass
$n(p)$	electron (hole) density
P	input optical flux
q	electron charge
R	reflectivity
R_L	load resistance
R_s	series resistance
$R_1(R_2)$	reflectivity of the surface (substrate) mirror in a resonant detector
T	temperature
t	time
$t_e(t_h)$	transit time for electrons (holes)
V_B	breakdown voltage
V_j	junction voltage
υ_e, υ_h	electron and hole velocities
W	thickness of the depleted region
x	position
α	absorption coefficient
α_{FC}	free carrier absorption inside the absorption layer
α_{FCx}	free carrier absorption outside the absorption layer
α_{IB}	interband absorption
α_i	electron ionization rate
α_s	scattering loss
β	propagation constant in a waveguide photodetector
β_i	hole ionization rate
Γ	confinement factor
ε	permittivity
η	quantum efficiency
κ	coupling coefficient to the waveguide of a waveguide detector
λ	wavelength
μ_e (μ_h)	mobility for electrons (holes)
ν	optical frequency
σ	charge density
σ_d	noise current spectral density
τ_e, τ_h	trapping time at a heterojunction for electrons (holes)
τ_{tr}	transit time
ϕ_{bc} (ϕ_{bv})	barrier height for the conduction band (valence band)
ω	angular frequency

HIGH-SPEED PHOTODETECTORS

26.2 INTRODUCTION

High-speed photodetectors are required for telecommunications systems, for high-capacity local area networks, and for instrumentation. Many different detector structures and materials are required to cover this range of applications. Silicon is one of the most commonly used detector materials for wavelengths from 0.4 to 1.0 μm, while Ge photodetectors are used at longer wavelengths up to 1.8 μm. Silicon and germanium have indirect bandgaps at these wavelengths, which result in relatively small bandwidth-efficiency products. Consequently, for high-speed applications, direct bandgap semiconductors such as III-V materials are more important and are the focus of this chapter. $Ga_{0.47}In_{0.53}As$ with a cutoff wavelength of 1.65 μm is especially useful for telecommunication photodetectors at 1.3 and 1.55 μm. GaAs has a cutoff wavelength around 0.9 μm and is ideal for visible and near-infrared applications.

This chapter will focus on the physics and technology of high-speed photodetectors. The next section discusses the different structures that are possible. Later sections discuss some specific results and motivations for particular structures. The primary limitations to detector speed are discussed, followed by a description of specific photodetector systems. To supplement this chapter, the reader should refer to excellent chapters and articles written specifically about photodetectors,[1] photoconductors,[2] pin detectors,[3] avalanche photodetectors,[4] phototransistors,[5] and receivers.[6,7]

26.3 PHOTODETECTOR STRUCTURES

Many photodetector structures have been demonstrated and many more structures are possible. In this section, we classify the different possible structures and identify a few of the trade-offs. The optimum structure for a given application depends on the required bandwidth, efficiency, saturation power, linearity, ease of integration, and leakage current.

There are four common types of photodetectors: (1) photovoltaic detectors, (2) photoconductive detectors, (3) avalanche photodetectors (APD), and (4) phototransistors. Photovoltaic detectors have blocking contacts and operate under reverse bias. The blocking contact can be a reverse-biased *p-n* junction or a Schottky contact. The photoconductive detector has identical, nonblocking contacts such as two *n*+ regions in an undoped sample. The avalanche photodetector has a similar configuration to a photovoltaic detector except that it has a high-field region that causes avalanching and results in gain in the detector. Improvements to the basic APD design include separate avalanche and gain regions (SAM APDs), and staircase APDs to increase the ratio of electron to hole (or hole to electron) multiplication rate. Phototransistors are three-terminal devices which have an integrated electronic gain region.

The second criterion is the contact type and configuration. The photogenerated carriers may be collected by means of (1) a vertical current collector, often a *p-n* or Schottky junction, (2) an interdigitated metal-semiconductor-metal (MSM) structure, or (3) a laterally grown or etched structure. These options are illustrated in Fig. 1*a*. PIN junctions are usually formed during the growth steps and tend to have low leakage current and high reliability.[8,9] Schottky junctions are simple to fabricate, but tend to have a large leakage current on narrow-gap semiconductors, such as InGaAs. MSM structures have the advantage of lower capacitance for a given cross-sectional area, but often have longer transit times, limited by the lithography capabilities possible in production. Experimental demonstrations with very fine lines (50 nm) have yielded high-speed devices with good quantum efficiencies. MSM detectors tend to be photoconductive detectors, but one could lower the capacitance for a given area of a PIN detector by using an interdigitated MSM structure with *p* and *n* regions under alternating metal fingers.

The third important aspect of photodetector design is the orientation of the light with respect to the wafer and the current collection region (Fig. 1*b*). Most commercial photodetectors are vertically illuminated and the device area is 10 μm in diameter or larger, which allows simple, high-yield packaging with single-mode optical fibers, or easy alignment to external bulk optics. The problem with this configuration is that the absorbing layer must be thin for a high-speed detector to keep

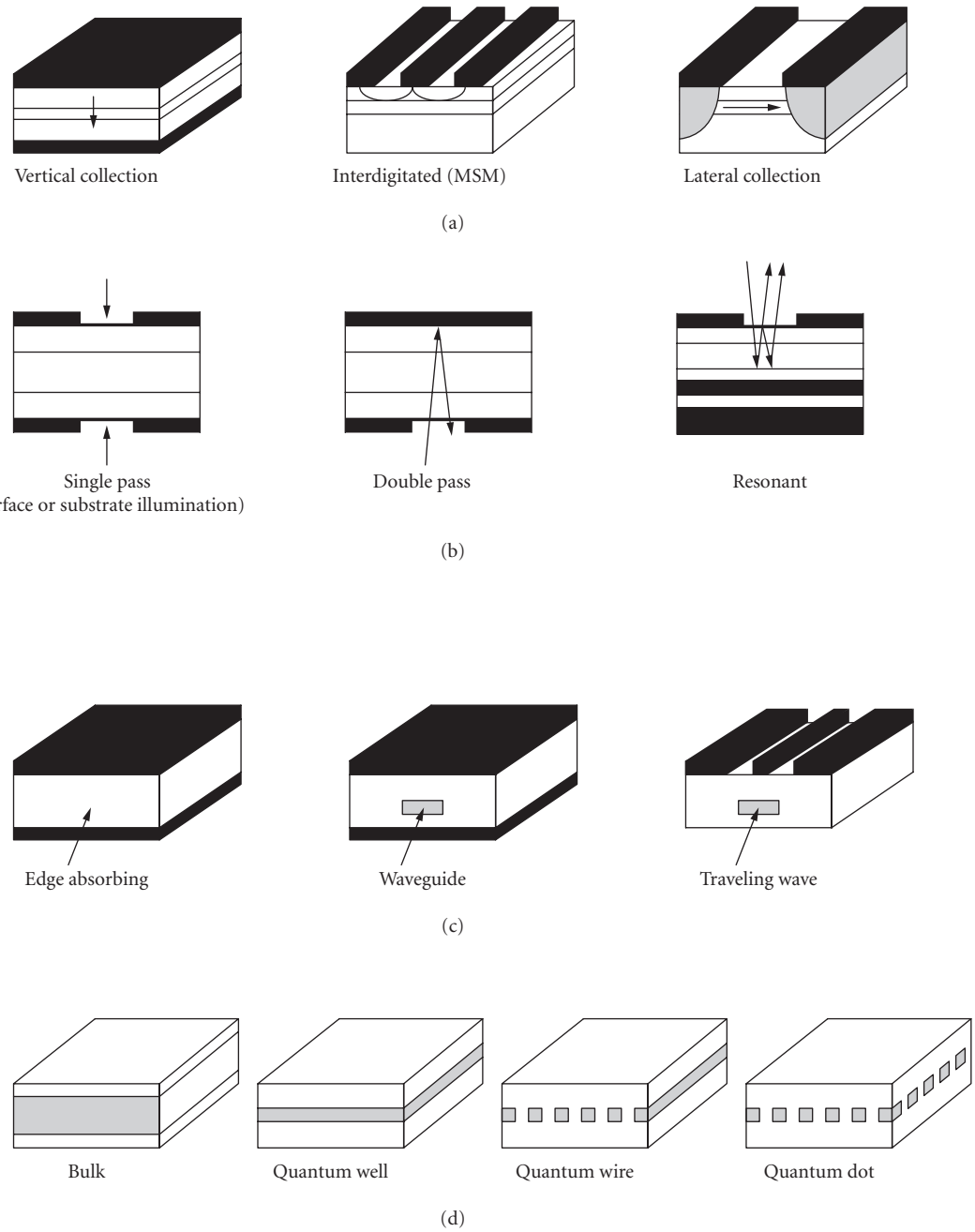

FIGURE 1 Schematic drawings of different types of photodetectors: (*a*) electrical configuration; (*b*) optical configuration—vertical illumination; (*c*) optical configuration—horizontal illumination; and (*d*) absorbing material.

the transit time of photogenerated carriers short. Consequently, the quantum efficiency is low, and single-pass vertically illuminated photodetectors tend to have bandwidth efficiency products around 30 GHz.[3] Bandwidth efficiency products are discussed in greater detail in Sec. 26.5. The bandwidth efficiency product can be increased by allowing two passes by reflecting the light off a metal layer or dielectric mirror.[10] Making a resonant cavity with multiple reflections at particular wavelengths should allow bandwidth efficiency products in excess of 100 GHz.[11–13] As will be seen below, essentially 100 percent quantum efficiency is possible with bandwidths up to 20 GHz, so there is no need for resonant detectors unless the required bandwidth is above 20 GHz or wavelength selectivity is needed as in a wavelength division multiplexed (WDM) system.

The other class of optical inputs are horizontally illuminated photodetectors (Fig. 1*c*). The simplest configuration is an edge-illuminated detector. The primary problem with an edge-illuminated detector is that the light is not guided. Diffraction of the incident light causes absorption to occur outside of the high-field region, and slow diffusion tails in the impulse response occur. A solution to this problem is the waveguide detector, where an optical waveguide confines the light to the high-field absorption region.[14–16] The waveguide efficiency product of this structure can be 100 to 200 GHz. However, it is limited by the capacitance of the structure, particularly if thin intrinsic layers are used for ultrahigh-speed devices. A solution to the capacitance limitation is a traveling wave photodetector where the incoming optical beam is velocity matched with the generated microwave signal.[17,18] The bandwidth efficiency product is then limited only by loss on the electrical transmission lines, and bandwidth efficiency products of hundreds of GHz are possible. Traveling wave detectors and, to a lesser extent, waveguide detectors have the important advantage that the volume of the light absorption can be quite large and, consequently, these detectors have much higher saturation powers.[19] Velocity matching in these structures requires quite narrow waveguides. Wu and Itoh[20] have suggested separating the parts of the optical waveguide with microwave delay lines to achieve velocity matching.

The fourth issue is the type of absorbing material (Fig. 1*d*) (1) bulk; (2) quantum well; (3) quantum wire; (4) quantum dot; (5 to 7) strained quantum well, wire, or dot; (8) *n-p-i-i* structure. The vast majority of commercial and experimental detectors use bulk material. However, quantum well detectors[21] are becoming increasingly important in photonic integrated circuits (PICs) because the absorbing quantum well material is also used in other parts of the PIC such as the laser. Quantum wire photodetectors[22] have potential advantages in terms of higher-bandwidth-efficiency products, but uniform quantum wires are rather difficult to fabricate. Quantum dot detectors have even higher peak absorption coefficients and more wavelength selectivity, but will probably have problems with slow impulse responses due to trapping of the carriers by the heterojunction. In other quantum-confined detectors, the carriers can be extracted along the quantum wire or well, and this problem can be avoided.[22]

The final classification is by means of the lifetime of the material. Conventional detectors have material lifetimes of typically 1 ns and achieve speed by using high field for rapid carrier collection. A second approach is to use low temperature (LT) grown material which has a very short lifetime, perhaps as low as 1 ps. A third approach is to damage the material by means of ion implantation. The final approach is to grow or diffuse in traps into the material such as iron[23] or gold.

If we combine these classifications, we find that 2600 types of photodetectors are possible, and additional subgroups such as superlattice APDs or SAGM APDs increase the total even further. In reality, about 100 types of detectors have been demonstrated. One of the points of this section is that improvements in one type of detector, such as adding a resonant cavity to a PIN detector, can be applied to other types of detectors, such as adding a resonant cavity to an APD. In the following section, we discuss in more detail some of the real limitations to the speed of a detector, and then apply this knowledge to a few important types of detectors.

26.4 SPEED LIMITATIONS

Generally speaking, the bandwidths of most photodetectors are limited by the following factors: (1) carrier transit time, (2) RC time constant, (3) diffusion current, (4) carrier trapping at heterojunctions, and (5) packaging. These limiting factors will be discussed in turn with specific application to *p-i-n* photodiodes.

Carrier Transit Time

In response to light absorbed in a material, the photogenerated carriers in the active region will travel across the high-field region and then be collected by the electrodes. As an example, Fig. 2*a* shows the *p-i-n* structure with a photogenerated electron-hole charge sheet of density σ. In response to the electric field, the electron will travel to the right and the hole to the left. This induces a

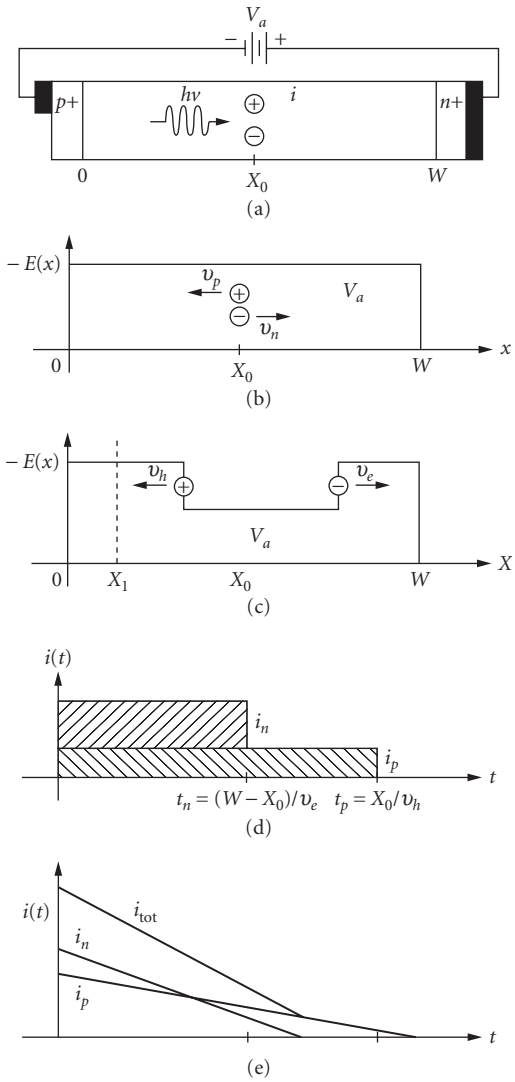

FIGURE 2 (*a*) Biased *p-i-n* structure. (*b*) Electrical field at the time when the electron-hole pairs are generated. (*c*) The perturbed electrical field due to the separated electron-hole pair. (*d*) The photocurrent due to single electron-hole pair. (*e*) The total photocurrent due to uniform illumination across the photodiode.

HIGH-SPEED PHOTODETECTORS

displacement current and reduces the internal electric field (Fig. 2*b* and *c*), which is the cause of saturation in photodetectors. From Gauss's law the difference in the electric field at the position of electron or hole is

$$\Delta E = \frac{q\sigma}{\varepsilon} \tag{1}$$

where q is the electron charge, and ε is the permittivity. Due to the constant total voltage across the depletion region, the reduced electric field between the electron and hole will be compensated by the increased electric field outside. The rate of change of the electric field at the position $X = X_1$ is

$$\frac{\partial E}{\partial t} = -\frac{(\upsilon_e + \upsilon_h)\Delta E}{W} \tag{2}$$

where υ_e and υ_h are the saturation velocities for electrons and holes, respectively. The assumption of saturation velocities is valid at high fields. The displacement current is hence given by

$$i(t) = -\varepsilon A\frac{\partial E}{\partial t} = \frac{qA\upsilon_e\sigma}{W} + \frac{q\upsilon_h\sigma A}{W} \tag{3}$$

The current consists of two components due to the electron and hole currents. The electron current lasts for a time duration of $(W - X_0)/\upsilon_e$ and hole current of X_0/υ_h. This is shown in Fig. 2*d*. Here, we note that if the fast carrier (i.e., electron) travels a longer distance, then we have a shorter pulse. The total electron and hole currents are given by

$$i_e(t) = \frac{q\upsilon_e A}{W}\int_0^w n(x,t)dx \tag{4}$$

$$i_h(t) = \frac{q\upsilon_h A}{W}\int_0^w p(x,t)dx \tag{5}$$

where $n(x, t)$ and $p(x, t)$ represent the electron and hole densities in the depletion region. The total current is the sum of Eqs. (4) and (5).

RC Time Constant

The RC time constant is determined by the equivalent circuit parameters of photodiode. For example, the intrinsic response of the *p-i-n* diode can be modeled as a current source in parallel with a junction capacitor. The diode series resistance, parasitic capacitance, and load impedance form the external circuit. Figure 3 shows the equivalent circuit of the *p-i-n* photodiode. The junction capacitance is defined by the edge of the depletion region (or space charge region). The series resistance is due to the ohmic contacts and bulk resistances. In addition, the parasitic capacitance depends on the metallization

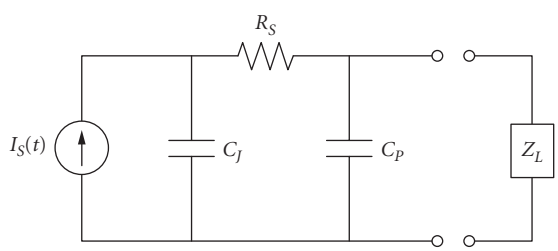

FIGURE 3 Equivalent circuit of a photodiode.

geometry. If the diode series resistance is R_s and a load resistance R_L is used to terminate the device, then the electrical 3-dB bandwidth can be approximated as

$$f_{3\text{dB}} = \frac{1}{2\pi(C_J + C_P)(R_L + R_S)} \tag{6}$$

If the photodiode is bonded by a section of gold wire, additional series inductance will be included in the load impedance. The 3-dB bandwidth due to parasitics in this case is then given in Ref. 3.

Diffusion Current

Diffusion current is important in detectors in which significant absorption occurs in regions outside the high-field region. This effect is reduced to some extent by recombination in these highly doped contact layers. Those carriers within about one diffusion length of the depletion region will have a chance to diffuse into the active region. This diffusion current will contribute a slow tail to the detector impulse response (Fig. 4). The electron diffusion current at the edge of the depletion region is given by

$$J_e = qD_e \frac{\partial n}{\partial x} = qD_e \frac{\Delta n}{L_e} \tag{7a}$$

and

$$J_h = -qD_h \frac{\partial p}{\partial x} = qD_h \frac{\Delta p}{L_h} \tag{7b}$$

where $D_e(D_h)$ and $L_e(L_h)$ are the diffusion coefficient and diffusion length, respectively, for electrons (holes). The diffusion process is a relatively slow process compared with the drift process. Assuming the photocarrier density is n, with the Einstein relation and Eq. (7*a*), the electron diffusion current can be written as

$$J_{\text{DIFF}} = qn\mu_e \left(\frac{kT/q}{L_e} \right) \tag{8}$$

and the drift current term for electron can be written as

$$J_{\text{DRIF}} = qn\mu_e \mathbf{E} \tag{9}$$

where μ_e is the electron mobility and $\mathbf{E}$ is the electric field. For most devices the electric field inside the depletion region is an order of magnitude larger than $(kT/q)L_e$. For example, the hole diffusion

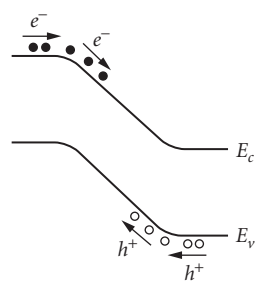

FIGURE 4 The origins of diffusion current.

HIGH-SPEED PHOTODETECTORS

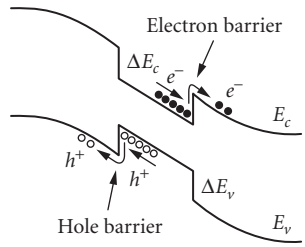

FIGURE 5 Heterostructure carrier trapping effect.

length for GaAs is typically around 10 μm and electric field is very often over 10 kV/cm. However, the diffusion-current terms could last as long as the carrier lifetime and the charge content in the tail can be as large as the drift component due to the slow diffusion times. For high-speed detectors, the diffusion-current problem can be eliminated with a double-heterostructure design that limits the absorbing regions to the high-field intrinsic regions.[24]

Carrier Trapping

Heterojunctions in photodetectors cause carrier trapping of electrons at conduction band discontinuities and trapping of holes at valence band discontinuities (Fig. 5). Hole trapping is a significant problem in long-wavelength photodetectors because of the large valence band discontinuity at the InP/InGaAs heterojunction. Usually, the emission rate is approximated by thermionic emission. If the interface deep-level recombination rate is significant, the total emission rate will be the sum of the two emission rates. The emission functions for electrons and holes are given by

$$e_n(t) = (1/\tau_e)\exp(-t/\tau_e)u(t) \tag{10a}$$

$$e_p(t) = (1/\tau_h)\exp(-t/\tau_h)u(t) \tag{10b}$$

where τ_e (τ_h) represents the emission time constant for electron (hole) and $u(t)$ is the step function. The rates of thermionic emission of trapped carrier are related to the Schottky barrier height due to the bandgap discontinuity:

$$1/\tau_e = B\exp(-\phi_{be}/kT) \tag{11}$$

where B is a constant and ϕ_{bc} is the barrier height for the conduction band. The response of the carrier-trap current in time domain is often obtained by convolving an intrinsic current source with the emission function. Since the applied bias will reduce the barrier height, sufficient device bias therefore will increase the emission rate. In order to reduce the barrier height, superlattice or compositional grading is often added at the heterointerface.[24]

Packaging

The external connections to the photodetector often limit the detector performance. Another problem is that the photodiode is a high impedance load and the device has a reflection coefficient close to unity. One solution to this problem is to integrate a matching resistor with the device.[24] This can usually be added using the lower contact layer without adding any additional mask or process steps. Figure 6 shows a Smith chart plot of the impedance of a typical photodetector along with the impedance of a device with an integrated matching resistor. A good match up to 40 GHz

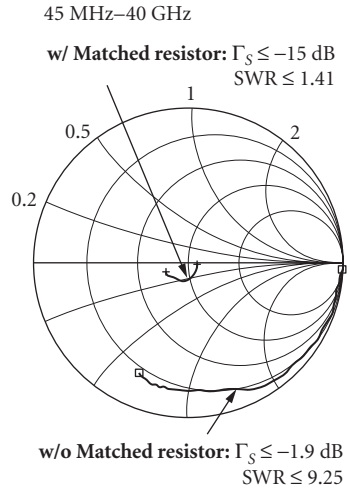

FIGURE 6 Smith chart of the impedance of typical photodiodes and photodiodes with integrated matching resistors.

is achieved. The disadvantage of a load resistor is the reduction in effective quantum efficiency by a factor of two since half of the photocurrent goes through the matching resistor. However, since the load resistance is now one-half, the RC time constant is also cut in half. Bandwidths in excess of 100 GHz have been achieved with quite large devices (7×7 μm^2) in this way. A second problem with very high speed devices is the difficulty in building external bias circuits without resonances in the millimeter range. The necessary bias capacitor and load resistor can be integrated with *p-i-n* photodetector without adding any additional mask or process steps by using a large-area *p-i-n* region as the capacitor and using the lower contact layer as the series resistor.[23] A photograph of the device is shown in Fig. 7 along with the device performance. In this case, bandwidths in excess of 100 GHz were achieved.

Optical fiber alignment and packaging are now quite standard. Simplified alignment by means of holes etched in the substrate of back-illuminated photodiodes may allow passive alignment of optical fibers. The photodetectors must be antireflection coated to reduce the reflection to air or optical epoxy. Single dielectric layers are typically used to minimize the reflection at one wavelength. Braun et al.[25] have achieved minimum reflectivity at multiple wavelengths with one dielectric layer by using one of the semiconductor layers in a multiple antireflectivity design.

26.5 *P-I-N* PHOTODETECTORS

Vertically Illuminated *p-i-n* Photodiode

In order to increase the frequency response of the vertically illuminated *p-i-n* photodiode, the efficiency is always sacrificed. As the active layer thickness is reduced, the transit time decreases, and the optical absorption decreases, and there is a trade-off between the efficiency and speed. The external quantum efficiency for a surface-illuminated *p-i-n* diode is given by

$$\eta = (1-R) \times (1-e^{-\alpha L}) \tag{12}$$

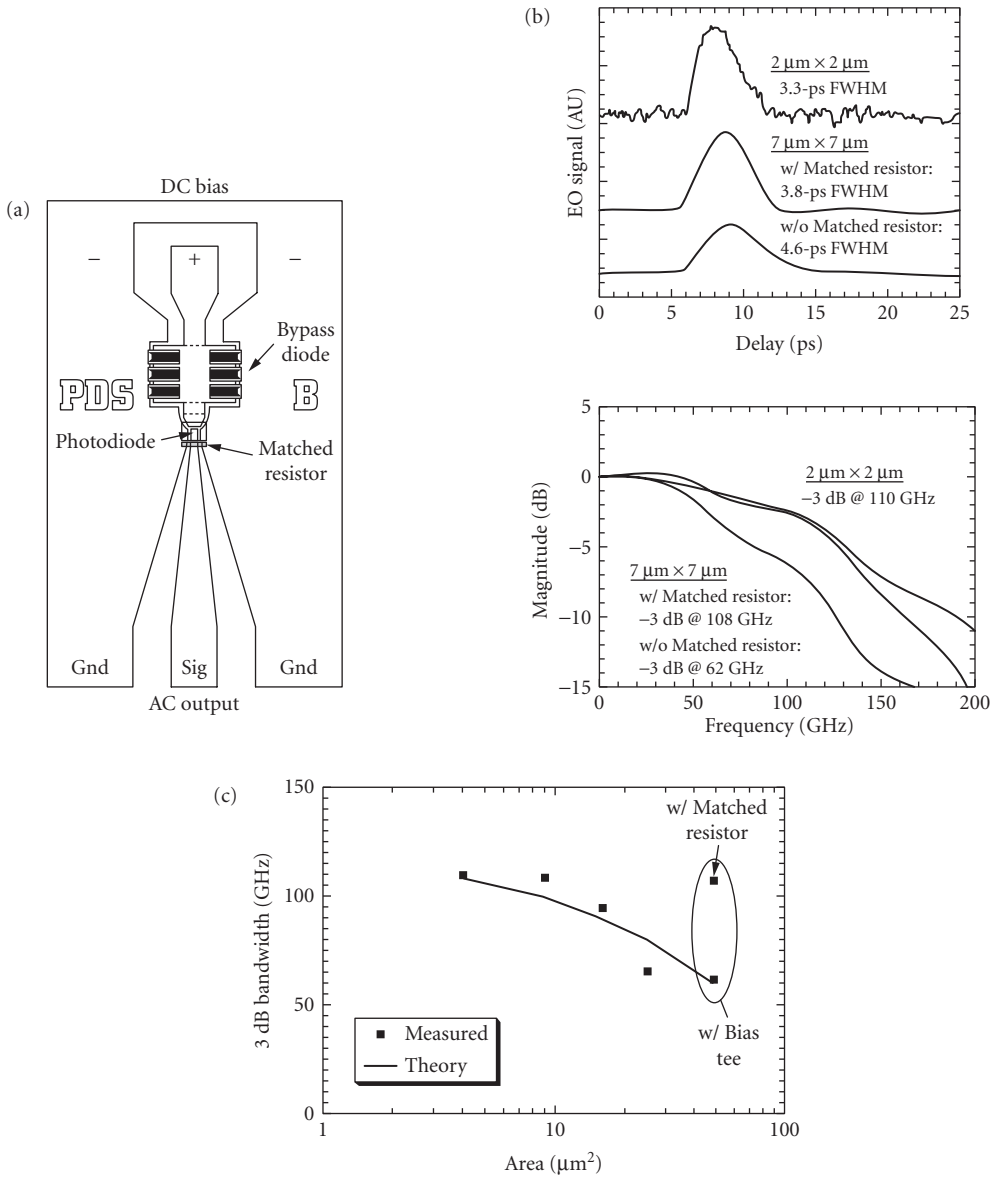

FIGURE 7 (*a*) Schematic diagram of a *p-i-n* photodiode with integrated matching resistor and bias circuit. (*b*) Impulse response of a 2×2 μm pin detector compared to 7×7 μm detectors with and without matching resistors. (*After Ref. 24.*) (*c*) Dependence of measured bandwidth on detector area and comparison to the theory presented in the text.

where R is the surface reflection, α is the absorption coefficient, and L is the active layer thickness. Since the absorption coefficient is a function of wavelength $\alpha = \alpha(\lambda)$, usually α decreases as λ increases. Thus, the diode intrinsic response is wavelength dependent. We can easily see the effect of light absorption on the transit-time-limited bandwidth by comparing the transit-time response[3,25] for two limiting cases for $\alpha L \to 0$ and $\alpha L \to \infty$ when $t_e = t_h = \tau_r$. The transit-time frequency response for a uniformly illuminated detector is

$$\left|F(\omega)_{\alpha L\to 0}\right| = \frac{2}{\omega\tau_{\text{tr}}}\left[1 + \frac{\sin^2\left(\frac{\omega\tau_{\text{tr}}}{2}\right)}{\left(\frac{\omega\tau_{\text{tr}}}{2}\right)} - 2\frac{\sin(\omega\tau_{\text{tr}})}{(\omega\tau_{\text{tr}})}\right]^{1/2} \tag{13}$$

For electron-hole pairs generated near the p side of the intrinsic region, electrons travel across the i region, and the frequency response is given by

$$\left|F(\omega)_{\alpha L\to\infty}\right| = \left|\frac{\sin\left(\frac{\omega\tau_{\text{tr}}}{2}\right)}{\left(\frac{\omega\tau_{\text{tr}}}{2}\right)}\right| \tag{14}$$

For these two limits, the transit-time-limited bandwidths are $f_{3\text{dB}(\alpha L=0)} = 0.45/\tau_{\text{tr}}$ and $f_{3\text{dB}(\alpha L=\infty)} = 0.55/\tau_{\text{tr}}$, respectively. For long-wavelength high-speed p-i-n diodes, the absorption layer is often very thin so that $1 - \exp(-\alpha L) \approx \alpha L$. The bandwidth efficiency product for transit-time-limited p-i-n diode is given by[3]

$$\eta f_{3\text{dB}} = 0.45\alpha v_s \tag{15}$$

Figure 8 shows the calculated 3-dB bandwidth for GaInAs/InP p-i-n diodes on the device area versus thickness plane for wavelength $\lambda = 1.3$ μm. The horizontal axis is the active layer thickness (which

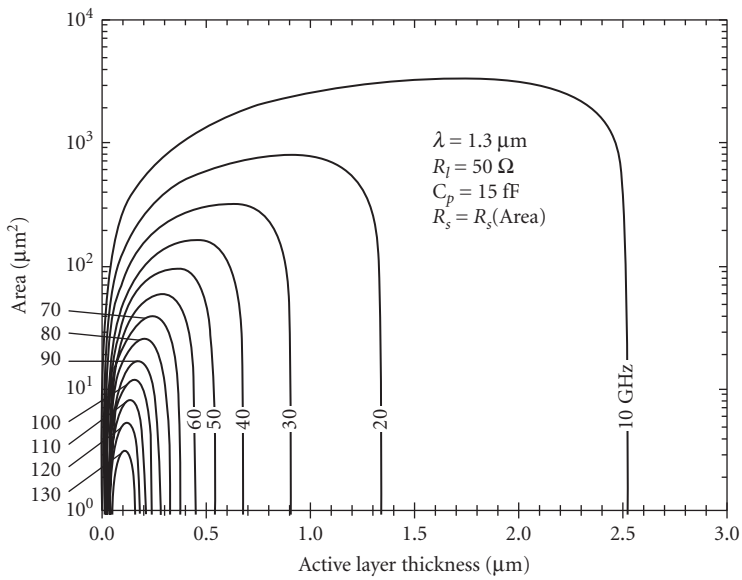

FIGURE 8 Calculated 3-dB bandwidth contours for a GaInAs pin vertically illuminated photodiode.

corresponds to the quantum efficiency) and the vertical axis is the device area. As we can see, when the device active layer thickness decreases, the quantum efficiency of *p-i-n* diode also decreases due to the insufficient light absorption in the active layer. The capacitance decreases as the device area decreases. Optimization of the device bandwidth is reached when transit-time-limited bandwidth approximately equals the RC limited bandwidth.

To minimize the bonding-pad capacitance, a semi-insulating substrate and thick polyimide layer are often used. Sometimes the series inductance of the bond wire is used to resonate the parasitic capacitance, and this results in a slightly peaked response with an increased 3-dB corner frequency. The electrical transfer function with series inductance is given by

$$H(\omega)=\frac{R_L}{[1-\omega^2(R_S R_L C_J C_P + L_S(C_J+C_P))]-j[\omega(R_L(C_J+C_P)+R_S C_J)-\omega^3 R_S C_J C_P L_S]} \tag{16}$$

where L_S is the series inductance.

To achieve high detector bandwidth, *double heterostructure* InP/GaInAs/InP *p-i-n* photodiodes have been fabricated to reduce the diffusion-current problem. However, carrier trapping can limit the impulse response. This effect can be characterized by the emission function $e_{e,h}(t)=(1/\tau_{e,h})\exp(-t/\tau_{e,h})$ where $\tau_{e,h}$ is emission time for electron (hole). The current-source response due to the electron and hole trapping at the heterointerfaces for *p*-side illumination is given by

$$\frac{i_s(\omega)}{i_s(0)}=\frac{1}{(1-e^{-\alpha L})}\left\{\left(\frac{1-e^{-j\omega t_e}}{j\omega t_e}-e^{-\alpha L}\frac{1-e^{-\alpha L}e^{-j\omega t_e}}{j\omega t_e-\alpha L}\right)\left(\frac{1}{1+j\omega\tau_e}\right)\right.$$
$$\left.+\left(\frac{1-e^{-\alpha L}e^{-j\omega t_h}}{j\omega t_e+\alpha L}-e^{-\alpha L}\frac{1-e^{-j\omega t_h}}{j\omega t_h}\right)\left(\frac{1}{1+j\omega\tau_h}\right)\right\} \tag{17}$$

and for *n*-side illumination is given by

$$\frac{i_s(\omega)}{i_s(0)}=\frac{1}{(1-e^{-\alpha L})}\left\{\left(\frac{1-e^{-\alpha L}e^{-j\omega t_e}}{j\omega t_e+\alpha L}-e^{-\alpha L}\frac{1-e^{-j\omega t_e}}{j\omega t_e}\right)\left(\frac{1}{1+j\omega\tau_e}\right)\right.$$
$$\left.+\left(\frac{1-e^{-j\omega t_h}}{j\omega t_h}-e^{-\alpha L}\frac{1-e^{-\alpha L}e^{-j\omega t_h}}{j\omega t_h-\alpha L}\right)\left(\frac{1}{1+j\omega\tau_h}\right)\right\} \tag{18}$$

where $\tau_{e,h}$ is the electron (hole) transit time. Other than the original *p-i-n* diode response, the extra terms $1/(1+j\omega\tau_{e,h})$ are due to the trapping effect. For InGaAs/InP heterostructure *p-i-n* diodes, the valence band offset is larger than the conduction offset and the hole effective mass is much larger than the electron effective mass. Thus, hole trapping is worse than the electron trapping in an InGaAs/InP *p-i-n* diode.

Waveguide *p-i-n* Photodiode

The main advantages of waveguide detectors are the very thin depletion region resulting in a very short transit time and the long absorption region resulting in a high bandwidth photodetector with a high saturation power (Fig. 1*c*). Due to the thin intrinsic layer, it can often operate at zero bias.[27] The absorption length of a waveguide detector is usually *designed to be long enough* (>5 μm) to ensure full absorption. The waveguide structure design (Fig. 9) is often required to have low coupling loss due to modal mismatch and reasonable effective absorption coefficient. The external quantum efficiency of a waveguide *p-i-n* detector is[28,29]

$$\eta=\kappa(1-R)\frac{\Gamma\alpha_{1B}}{\alpha}(1-e^{\alpha L}) \tag{19}$$

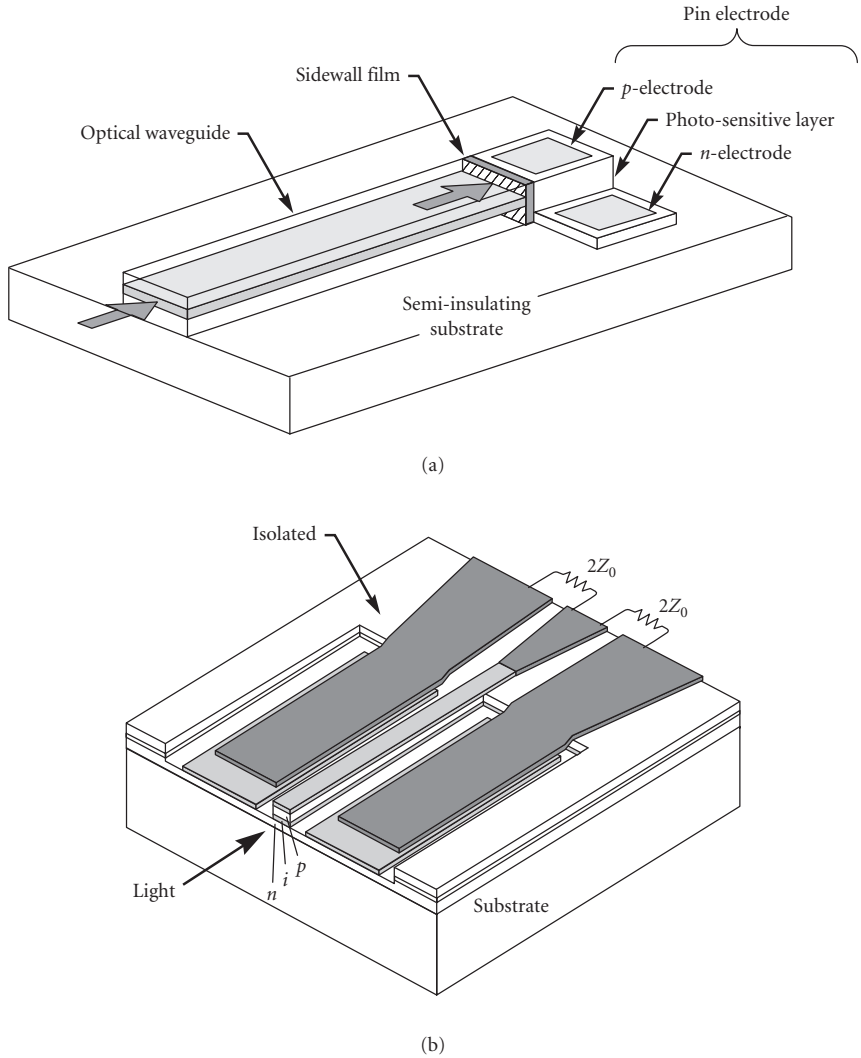

FIGURE 9 Schematic diagram of (*a*) a waveguide photodetector (*after Ref. 14*) and (*b*) a traveling wave photodetector (*after Ref. 17*).

where κ is the coupling efficiency due to the modal mismatch, Γ is the mode confinement factor, α_{IB} is the interband absorption. The loss coefficient α is given by

$$\alpha = \Gamma\alpha_{\mathrm{IB}} + \Gamma\alpha_{\mathrm{FC}} + (1-\Gamma)\alpha_{\mathrm{FCx}} + \alpha_s \tag{20}$$

where α_{FC}, α_{FCx} are the free carrier absorption loss inside and outside the absorption layer, α_s is the scattering loss. Kato et al.[14] reported an InGaAs waveguide *p-i-n* diode with bandwidth of 40 GHz. The detector quantum efficiency is 44 percent at 1.55-μm wavelength. The coupling loss estimated by an overlap integral was 2.1 dB. To reduce the coupling loss, it is important to have a good design of the layer structure to reduce modal mismatch and to coat the facet with an antireflecting (AR) film.

Resonant *p-i-n* Photodiode

A resonant detector utilizes the multiple passes in a Fabry-Perot resonator to achieve high quantum efficiency with thin absorbing layers (Fig. 1*b*). Since the speed of light is about three orders of magnitude faster than the carrier velocities, the quantum efficiency can be increased without significant pulse broadening due to the effective optical transit time.

The schematic diagram of a resonant cavity-enhanced photodetector is shown in Fig. 10. The efficiency of the resonant detector is given by

$$\eta = \left[\frac{(1+R_2 e^{-\alpha d})}{1-2\sqrt{R_1 R_2}\, e^{-\alpha d}\cos(2\beta L+\phi_1+\phi_2)+R_1 R_2 e^{-2\alpha d}} \right] \times (1-R_1)\times(1-e^{-\alpha d}) \tag{21}$$

where R_1, R_2 are mirror reflectivities, ϕ_1, ϕ_2 are mirror phase shifts, $\beta = 2\pi/n\lambda$ is the propagation constant, and d is the thickness of active region. The quantum efficiency has its maximum when $2\beta L+\phi_1+\phi_2 = 2m\pi$ (m=1, 2, 3, ...) and the quantum efficiency is then

$$\eta = \left[\frac{(1+R_2 e^{-\alpha d})}{(1-\sqrt{R_1 R_2}\, e^{-\alpha d})^2} \right] \times (1-R_1)\times(1-e^{-\alpha d}) \tag{22}$$

Figure 11 shows the calculated resonant quantum efficiency versus normalized absorption coefficient αd.[11] High quantum efficiency is possible even from thin absorption layers.

However, in terms of the fabrication, the material growth, and the structure design, building a high-speed resonant photodetector is not a simple task. The required low resistance and low capacitance with incorporated mirror structure is difficult to achieve due to the significant resistance of the multiple heterojunction mirror stack.

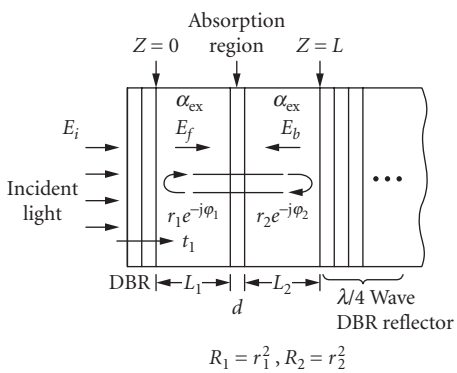

FIGURE 10 Schematic diagram of a resonant photodetector. (*After Ref. 13.*)

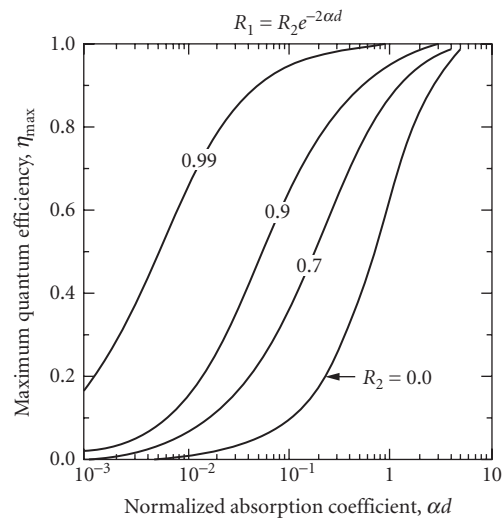

FIGURE 11 Dependence of quantum efficiency on mirror design in a resonant photodetector. (*After Ref. 13.*)

26.6 SCHOTTKY PHOTODIODE

Schottky photodiodes[30–32] are especially attractive for integration with FETs and III-V integrated circuits because of their simple material structure and easy fabrication. Figure 12 shows the Schottky barrier structure. For front-illuminated devices, the metal is very thin so that the light can penetrate the metal with very little loss. The *J-V* characteristic of a Schottky diode is given by[33]

$$J = J_0\left[\exp\left(\frac{qV}{k_BT}\right)-1\right] \tag{23}$$

where

$$J_0 = A^{**}T^2\exp\left(-\frac{q\Phi_b}{k_BT}\right) \tag{24}$$

and ϕ_b is the barrier height and A^{**} is the modified effective Richardson constant.[34]

The dynamics of photogenerated carriers in a Schottky diode are similar to those of a *p-i-n* diode (Fig. 2). The dynamics of both electrons and hole must be included in the analysis of a Schottky photodiode, resulting in expressions for the Schottky diode response given in Eqs. (13) to (18) with the exception that there is no diffusion current from the metal layer. The equivalent circuit of a Schottky diode is the same as that of a *p-i-n* diode.

In high-speed applications, GaAs Schottky diodes in the short-wavelength region with bandwidths over 200 GHz have been reported.[36] These devices can be combined with FETs or sampling diodes.[35,36] Figure 13 shows an integrated Schottky photodiode with a diode sampling circuit. A pair of short voltage pulses are generated by the nonlinear transmission line and a differentiator. The short voltage pulses are used to control the sampling capacitors to measure the photodiode signal. The sampled signal is then passed through a low-pass filter to extract the equivalent time domain waveform. Impulse responses of under 2 ps have been demonstrated in this way.[36]

In the long-wavelength region, GaInAs Schottky diodes experience high dark current problems due to the relatively low Schottky barrier height at the metal/GaInAs interface.[37] An InP or quaternary layer is usually added at the interface in order to increase the Schottky barrier height.[38] A graded bandgap layer (e.g., GaInAsP) is then needed at the GaInAs/InP interface to reduce hole trapping.

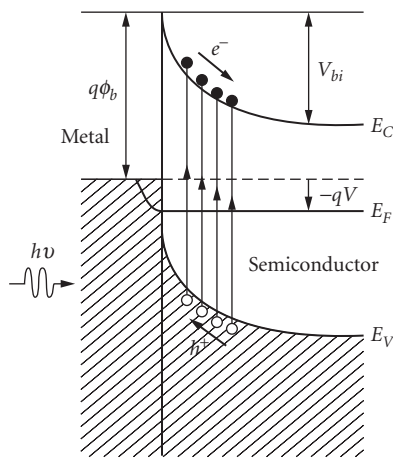

FIGURE 12 Schematic diagram of a Schottky barrier photodiode.

HIGH-SPEED PHOTODETECTORS

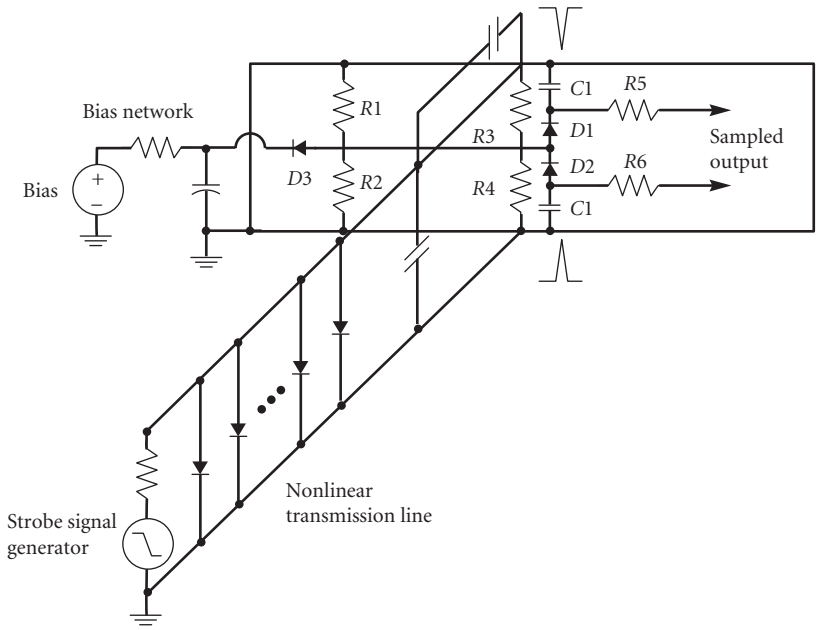

FIGURE 13 Integrated Schottky photodiode and sampling circuit. (*After Ref. 35.*)

26.7 AVALANCHE PHOTODETECTORS

High-speed avalanche photodetectors (APDs) are widely used in fiber communication. APDs with gain-bandwidth (GB) products in excess of 100 GHz have been reported.[39–43] In long-wavelength applications, InGaAs/InP APDs are better than Ge APDs due to their lower dark current and lower multiplication noise. The Ge APD also has a limited spectral response at 1.55-μm wavelength. The maximum achievable GB product of InGaAs/InP APDs is predicted to be around 140 GHz,[44] while the gain-bandwidth product of Si APDs in the near-infrared region can have GB products of over 200 GHz.[45] InGaAs/InAlAs superlattice avalanche photodiodes have a lower ionization ratio ($k = 0.2$)[46] than bulk avalanche photodiodes, and lower noise and higher gain-bandwidth product can be achieved.

High-speed GaInAs/InP APDs make use of separated absorption and multiplication layers (SAM APD). Figure 14 shows the simplified one-dimensional APD structure. The narrow bandgap *n*-GaInAs layer absorbs the incident light. The layer is usually thick (>1 μm) to ensure high quantum efficiency. The electric field in the absorption layer is high enough for carriers to travel at saturated velocities, yet is below the field where significant avalanching occurs and the tunneling current is negligible. The wide bandgap InP multiplication layer is thin (a few tenths of a micron) to have shorter multiplication buildup time.[47,48] The bias is applied to the fully depleted absorption layer in order to obtain effective carrier collection efficiency and, at the same time, electric field in the multiplication region must be high enough to achieve avalanche gain. A guard ring is usually added to prevent premature avalanche breakdown (or microplasma) at the corner of the diffusion edge. To reduce the hole pileup effect, a graded bandgap layer (e.g., superlattice or compositional grading) is often added at the heterointerface between the absorption layer and multiplication layer. This is the so-called separated absorption, grading, multiplication avalanche photodiode (SAGM APD).

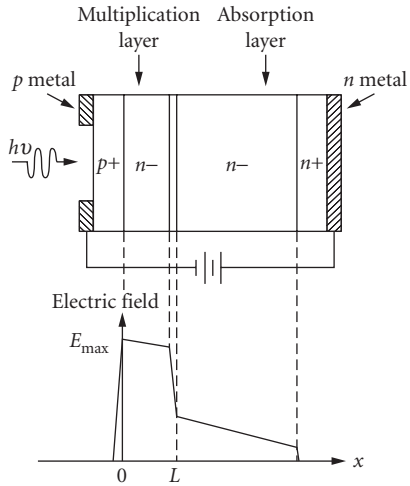

FIGURE 14 Schematic diagram of a SAGM APD.

The multiplication process in APDs can be described by the electron and hole ionization coefficients α_i and β_i. The field dependencies of ionization coefficients for electrons and holes are given by

$$\alpha_i(x) = A_e \exp(-B_e/E(x)) \tag{25a}$$

$$\beta_i(x) = A_h \exp(-B_h/E(x)) \tag{25b}$$

where $A_{e,h}$ and $B_{e,h}$ are constant parameters.[49] Since the electric field is generally position-dependent, the ionization coefficients are also position-dependent. With Eq. (25*a*, *b*) and the electric field distribution, the position-dependence of ionization coefficients can be derived. The multiplied photocurrent in the avalanche region ($0 \le x \le W$) including injected electron current density $J_n(0)$, injected hole current density $J_p(0)$, and photo-generation of electron-hole pairs $g(x)$ was derived by Lee et al.[50] The total photocurrent density is given by

$$J = \frac{J_p(w)\exp\left[-\int_0^w(\alpha_i-\beta_i)dx\right] + J_n(0) + q\int_0^w g(x)\exp\left[-\int_0^x(\alpha_i-\beta)dx'\right]dx}{1-\int_0^w \alpha_i \exp\left[-\int_0^w(\alpha_i-\beta_i)dx'\right]dx} \tag{26}$$

The electron-initiated and hole-initiated multiplication factors, M_n and M_p, can be obtained by putting $J_p(w) = g(x) = 0$ and $J_n(0) = g(x) = 0$, respectively in Eq. (26):

$$M_n = \frac{J}{J_n(0)} = \frac{1}{1-\int_0^w \alpha_i \exp\left[-\int_0^w(\alpha_i-\beta_i)dx'\right]dx} \tag{27a}$$

$$M_p = \frac{J}{J_p(w)} = \frac{\exp\left[-\int_0^w(\alpha_i-\beta_i)dx\right]}{1-\int_0^w \alpha_i \exp\left[-\int_0^w(\alpha_i-\beta_i)dx'\right]dx} \tag{27b}$$

The bandwidth of an APD is limited by the device RC time constant when the multiplication gain M is low (i.e., $M < \alpha_i/\beta_i$). As the multiplication gain increases above the ratio of the electron and hole ionization coefficients (i.e., $M > \alpha_i/\beta_i$), the avalanche buildup time becomes the dominant limitation on 3-dB bandwidth and the product of the multiplication gain and 3-dB bandwidth reaches a constant. The multiplication factor M as a function of frequency was derived by Emmons[51] and is given by

$$M(\omega) \approx \frac{M_o}{\{1+\omega^2 M_0^2 \tau_1^2\}^{1/2}}, \quad M_o > \alpha_i/\beta_i \tag{28a}$$

$$\tau_1 \approx N(\alpha_i/\beta_i)\tau \tag{28b}$$

where τ_1 is the effective transit time, τ is the multiplication-region transit time, and $N(\beta_i/\alpha_i)$ is a number changing between 1/3 and 2 as β_i/α_i varies from 1 to 10^{-3}. The dc multiplication factor M_o is given by Miller:[52]

$$M_o = \frac{1}{1-(V_j/V_B)^n} \tag{29}$$

where V_B is the breakdown voltage, V_j is the junction voltage, and n is an empirical factor ($n < 1$).

The total APD dark current consists of two components. I_{du} is the unmultiplied current which is mainly due to the surface leakage current. I_{dm} is the bulk dark current experiencing the multiplication process. The total dark current is expressed by

$$I_d = I_{du} + MI_{dm} \tag{30}$$

where M is the avalanche gain. The noise current spectral density due to the dark current is given by

$$\sigma_d^2 = 2qI_{du} + 2qI_{dm}M^2F(M) \tag{31}$$

where $F(M)$ is the avalanche excess noise factor derived by McIntyre.[53] Excess noise factors for electron-initiated or hole-initiated multiplication are given by

$$F(M) = F_e(M) = [kM + (1-k)(2-1/M)] \tag{32a}$$

$$F(M) = F_h(M) = \left[\frac{1}{k}M + \left(1-\frac{1}{k}\right)(2-1/M)\right] \tag{32b}$$

where k is the ratio of the ionization coefficient of holes to electrons ($k = \beta_i/\alpha_i$), and k is assumed to be a constant independent of the position. Figure 15 shows the sensitivity of an APD receiver as a function of k_{eff} which is obtained by weighting the ionization rates over the electric field profile. From Fig. 15 we can see that the smaller the k factor is, the smaller the noise factor is and the better the receiver sensitivity is. Ge APDs have k values close to unity (0.7 to 1.0). GaInAs/InP APDs using an InP multiplication region have $1/k$ values from 0.3 to 0.5. Silicon is an excellent APD material since its k value is 0.02. Therefore, a Si APD has an excellent low dark current noise density and is predominantly used at short wavelengths compared with Ge APDs and GaInAs/InP APDs which are used at longer wavelengths.

In optical receiver applications,[54,55] the photodetector is used with a low-noise amplifier. The dark current noise power is given by

$$\langle i_{nd}^2 \rangle = 2qI_{du}BI_2 + 2qI_{dm}M^2F(M)BI_2 \tag{33}$$

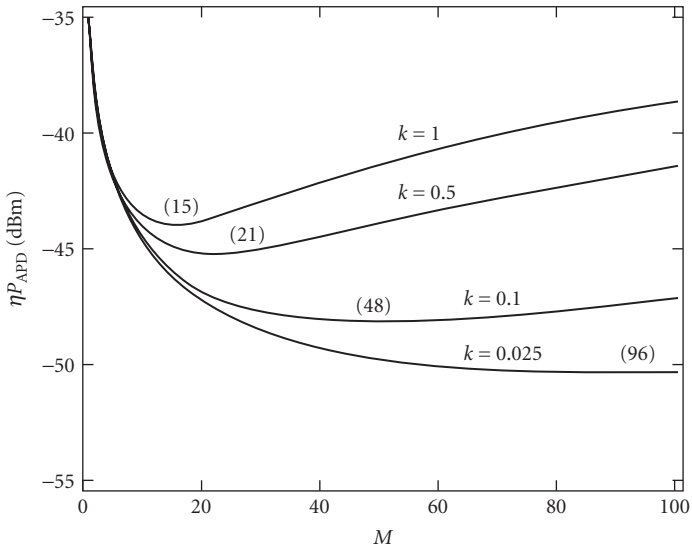

FIGURE 15 Dependence of APD receiver sensitivity on β/α in SAGM APDs. (*After Ref.* 7.)

where B is the receiver bit rate and I_2 is a parameter depending on the input optical pulse shape. The receiver sensitivity penalty[56] is given in terms of parameter ε_N.

$$\eta\bar{P} = (1+\varepsilon_N)\eta\bar{P}_o \tag{34}$$

where $\eta\bar{P}_o$ is the sensitivity with zero dark current. For example, $\varepsilon_N = 0.023$ for a 0.1-dB penalty. The maximum allowable dark current for a given sensitivity for a *p-i-n* FET receiver is

$$I_{du} = \frac{\varepsilon_N(2+\varepsilon_N)}{2qBI_2}\langle i_{na}^2 \rangle \tag{35}$$

where $\langle i_{na}^2 \rangle$ is the amplifier noise power and is proportional to B^3 above 100 MBits/s. Therefore, the maximum allowable dark current is proportional to B^2. For APD receivers, the maximum allowable dark current I_{dm} as a function of bit rate can be approximated by assuming that the sensitivity penalty is within 1 or 2 dB and optimum gain is constant. In Fig. 16, as we can see, the dark current is proportional to B at lower bit rates and $B^{1.25}$ at higher bit rates. So, as the bit rate increases, the maximum allowable dark current increases.

26.8 PHOTOCONDUCTORS

High-speed photoconductors[57–62] have become more important not only because of their simplicity in fabrication and ease of integration with MESFET amplifiers but also because of their useful applications for photodetector and photoconductor sampling gates. Usually the photoconducting film has a high density of defects with the trap energy levels deep within the bandgap to shorten the material lifetime and the detector impulse response. The characteristics of the photoconductive films include (1) high resistivity due to the fact that Fermi level is pinned at the midgap, (2) enhanced optical absorption for photon energy below the bandgap due to the introduction of new bandgap states, and (3) easy fabrication of ohmic contacts possibly due to the enhancement of tunneling through the narrow Schottky barrier with a pinned Fermi level.

HIGH-SPEED PHOTODETECTORS

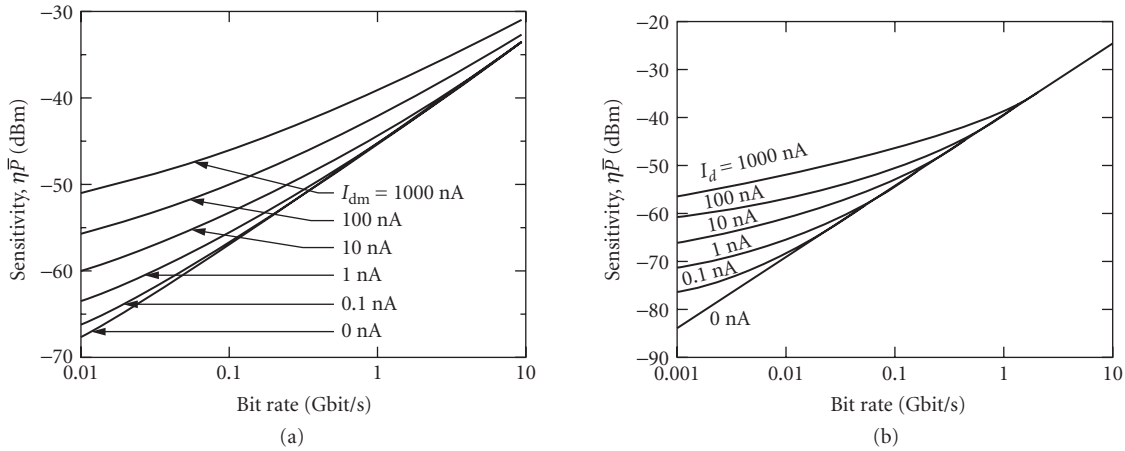

FIGURE 16 Dependence of receiver sensitivity on dark current for an (*a*) SAGM APD and (*b*) PIN detector, each with a GaAs FET preamplifier. (*After Ref. 6.*)

Figure 17 shows a typical photoconductor on a microstrip line structure. The photoconductive film is formed on top of a semi-insulating substrate. A microstrip transmission line consists of microstrip electrodes on top and ground plane on bottom. Under a steady-state illumination, the photogenerated carrier will experience high electrical field and travel to the electrodes. The photocurrent is

$$I_{\text{ph}} = \frac{q\eta GP}{h\nu} \tag{36}$$

where η is the external quantum efficiency, G is the photoconductor gain, and P is optical input flux. The photoconductor gain G is given by

$$G = \frac{\tau}{\tau_{\text{tr}}} \tag{37}$$

which is the ratio of carrier lifetime τ to the carrier transit time τ_{tr}. The frequency response of a photoconductive detector is plotted in Fig. 18 for different material lifetimes. In a detector without damage sites, the gain can be quite large at low frequencies. We can see from this figure how the

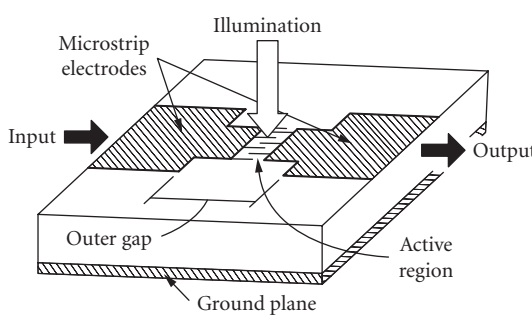

FIGURE 17 Schematic diagram of a high-speed photoconductor.

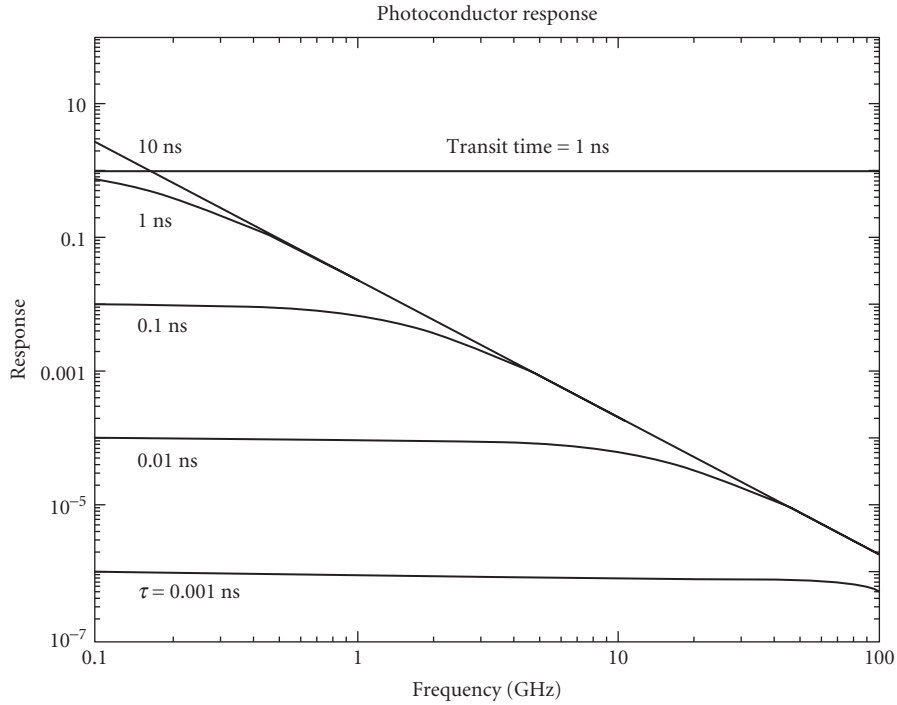

FIGURE 18 Frequency response of a photoconductor.

increased bandwidth is achieved at the expense of quantum efficiency. Using smaller finger separations, higher quantum efficiency can be achieved for a particular bandwidth.

The standard microstrip line configuration has reflection problems in the thickness direction of the substrate and the dispersion characteristics of a microstrip line is worse than that of a coplanar stripline.[57] Coplanar striplines with "sliding-contact" excitation can have zero capacitance to first order.[58] The photoconductor using coplanar stripline has been very successful in generating short electrical pulses. To measure the short electric pulse, several techniques can be used such as photoconductor sampling or electro-optic sampling. Both of the above techniques can provide subpicosecond resolution. The coplanar strip line configuration with sliding contact and sampling gate is shown in Fig. 19*a*. The equivalent circuit is shown in Fig. 19*b*.[58] The infinite capacitances represent that the line extends without end in both directions. The generated electrical signal due to the time-varying resistance $R_s(t)$ is

$$V_{\text{out}}(t) = V_b \frac{Z_o}{Z_o + R_s(t) + R_c} \tag{38}$$

where R_c is the contact resistance. If the excitation intensity is sufficiently low to keep $R_s(t) >> Z_o$, then

$$V_{\text{out}}(t) = V_b \frac{Z_o}{R_s(t) + R_c} \tag{39}$$

The photoconductor resistance $R_s(t)$ can be related to the photoexcited electron-hole pair density $n(t)$:[59]

$$R_s(t) = \frac{L}{qn(t)(\mu_e + \mu_e)wd_e} \tag{40}$$

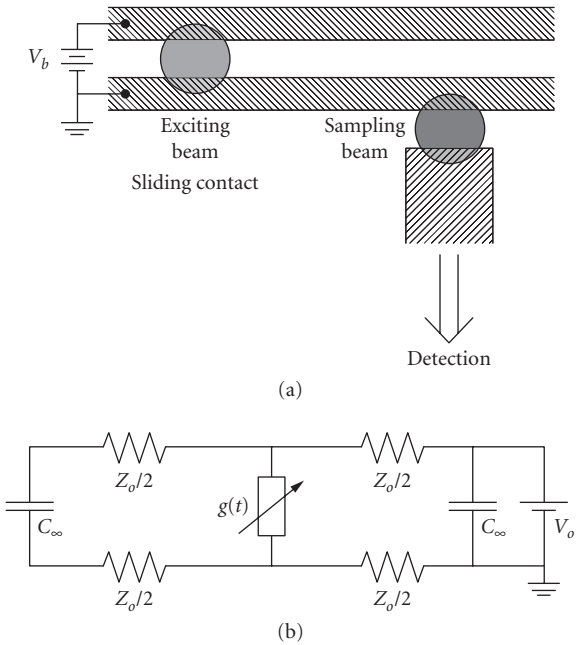

FIGURE 19 (*a*) Coplanar circuit layout of a photoconductor with sliding contact and (*b*) Equivalent circuit.

where L is the gap width, w is the width of photoconductive volume and d_e is the effective absorption length. When the pulse width is of the same order of magnitude as carrier lifetime and much shorter than the carrier transit time across the switch gap, the electron-hole pair density is given by

$$n(t) = e^{-t/\tau} \int_0^t e^{t/\tau} \frac{\eta P_o(t)(1-R)}{h\nu w d_e} dt \tag{41}$$

Here, we notice that the carrier density is an exponential decay function, so $G(t) = 1/R_s(t)$ is also an exponential decaying function with a time constant τ. This can be explained as a result of the convolution of the laser pulse with an exponential function with carrier life time τ.

The low temperature (LT) grown GaAs[60] can have both high carrier mobility and subpicosecond carrier lifetime when being compared with that of the ion-implanted photoconductor.[61] The dislocation density in LT GaAs is about the same as that in GaAs epitaxial layer grown at normal substrate temperatures such that the LT GaAs has a mobility as high as that of the bulk material. The resistivity of the LT GaAs is greater than that of semi-insulating GaAs ($>10^{17}$ Ω-cm) due to its high deep-level concentration. The LT GaAs photoconductive-gap switch in a coplanar strip transmission line configuration has obtained a 1.6-ps (FWHM) response with a 3-dB bandwidth of 220 GHz. Chen et al.[62] reported a high-speed photodetector utilizing LT GaAs MSM photoconductor. To achieve reasonable quantum efficiency and high-speed response, the optimum design requires carrier transit time approximately equal to carrier lifetime. With this requirement, the carriers not collected fast enough by the electrodes will be consumed by recombination. The response of a 0.2-μm finger and space MSM photodetector was measured by electro-optic sampling system. A 1.2 ps (FWHM) response with a 3-dB bandwidth of 350 GHz is obtained.

26.9 SUMMARY

Photodetector performance has steadily improved over the past decade. High-speed detectors are now available at a variety of wavelengths from 1.65 to 0.4 μm. MSM photoconductors have demonstrated the shortest impulse responses of under a picosecond. For applications that require high speed and high efficiency, the best results have been obtained using two passes through a *p-i-n* photodetector (30 percent quantum efficiency with 110-GHz bandwidth). Many applications require a high saturation power, and waveguide photodetectors have achieved the best results (20-GHz bandwidth with 0.5-A/W responsivity and 10-mW saturation power). Traveling wave photodetectors appear to offer the ultimate results in high-speed, high-responsivity, high-saturation power detectors. The combination of high-speed photodetectors with optical amplifiers is resulting in superb sensitivity of all bit rates, but requires the fabrication of high-speed photodetectors with at least 10-dBm saturation power.

An increasing amount of attention is being paid to integrating high-speed photodetectors with electronic and photonic circuits. Integration with electronic circuits increases the performance by eliminating the parasitics and limited bandwidth of bonding pads, wires, and connectors. Integration with optical waveguides decreases the optical loss associated with coupling from one device to another and reduces the packaging cost. Integration of photodetectors with optical amplifiers and wavelength tuning elements is a particularly important research direction.

26.10 REFERENCES

1. T. P. Lee and T. Li, "Photodetectors," *Optical Fiber Telecommunications,* S. E. Miller and A. G. Chynoweth (eds.), Academic Press, New York, 1979.
2. D. H. Auston, *Picosecond Optoelectronic Devices,* chap. 4, C. H. Lee (ed.), Academic Press, New York, 1984, pp. 73–117.
3. J. E. Bowers and C. A. Burrus, Jr., "Ultrawide-Band Long-Wavelength *p-i-n* Photodetectors," *J. Lightwave Tech.,* vol. LT-5, no. 10, October 1987.
4. F. Capasso, "Physics of Avalanche Photodiodes," *Semiconductors and Semimetals,* 22D, W. T. Tsang (ed.), Academic Press, New York, 1985.
5. J. Campbell, *Semiconductors and Semimetals,* 22D, W. T. Tsang (ed.), Academic Press, New York, 1985.
6. B. Kasper, "Receiver Design," *Optical Fiber Telecommunications II,* S. E. Miller and I. P. Kaminow (eds.), Academic Press, Boston, 1988.
7. S. R. Forrest, "Avalanche Photodetector Receiver Sensitivity," *Semiconductors and Semimetals,* vol. 22D, *Lightwave Communications Technology: Photodetectors,* W. Tsang (ed.), Academic Press, New York, 1985.
8. S. R. Sloan, "Processing and Passivation Techniques for Fabrication of High Speed InP/InGaAs/InP Mesa Photodetectors," *Hewlett Packard Journal,* Oct. 1989, p. 69.
9. K. Carey, S. Y. Wang, J. S. C. Chang, and K. Nauka, "Leakage Current in GaInAs/InP Photodiodes Grown by OMVPE," *J. Crystal Growth*, vol. 98, 1989, p. 90.
10. Y. G. Wey, D. L. Crawford, K. Giboney, J. E. Bowers, M. J. Rodwell, P. Silvestre, M. J. Hafich, and G. Y. Robinson, "Ultrafast Graded Double-Heterostructure GaInAs/InP Photodiode," *Appl. Phys. Lett.*, vol. 58, no. 19, 1991, p. 2156.
11. M. S. Unlu, K. Kishino, J. Chyi, L. Aresenault, J. Reed, and S. N. Mohammad, "Resonant Cavity Enhanced AlGaAs/GaAs Heterojunction Phototransistors with an Intermediate InGaAs Layer in the Collector," *Appl. Phys. Lett.,* vol. 57, no. 8, 20 Aug. 1990, p. 750.
12. A. Chin and T. Y. Chang, "Enhancement of Quantum Efficiency in Thin Photodiodes through Absorptive Resonance," *J. Lightwave Tech.,* vol. 9, no. 3, March 1991, p. 321.
13. K. Kishino, M. S. Unlu, J-I. Chyi, J. Reed, L. Arsenault, and H. Morkoc, "Resonant Cavity-Enhanced (RCE) Photodetectors," *IEEE J. Quantum Electron.,* vol. 27, no. 8, Aug. 1991, p. 2025.
14. K. Kato, S. Hata, A. Kozen, J. Yoshida, and K. Kawano, "High-Efficiency Waveguide InGaAs Pin Photodiode with Bandwidth of over 40 GHz," *IEEE Photon. Tech. Lett.,* vol. 3, no. 5, May 1991, p. 473.
15. D. Wake, S. N. Judge, T. P. Spooner, M. J. Harlow, W. J. Duncan, I. D. Henning, and M. J. O'Mahony, "Monolithic Integration of 1.5 μm Optical Preamplifier and PIN Photodetector with a Gain of 20 dB and a Bandwidth of 35 GHz," *Electron. Lett.,* vol. 26, no. 15, July 19, 1990, pp. 1166–1168.

16. R. J. Deri, N. Yasuoka, M. Makiuchi, H. Hamaguchi, O. Wada, A. Kuramata, and R. J. Hawkins, "Integrated Waveguide/Photodiodes with Large Bandwidth and High External Quantum Efficiency," *IEEE Photon. Technol. Lett.,* vol. 2, 1990, pp. 496–498.
17. K. S. Giboney, M. J. W. Rodwell, and J. E. Bowers, "Travelling-Wave Photodetectors," *Photon. Tech. Lett.,* vol. 4, no. 12, Dec. 1992, pp. 1363–1365.
18. H. Taylor, O. Eknoyan, C. S. Park, K. N. Choi, and K. Chang, "Traveling Wave Photodetectors," *SPIE Proc. on Optoelectronic Signal Processing for Phased Array Antennas II,* 1990, p. 59.
19. A. R. Williams, A. L. Kellner, X. S. Jiang, and P. K. L. Yu, "InGaAs/InP Waveguide Photodetector with High Saturation Intensity," *Electron. Lett.*, vol. 28, 1992, p. 2258.
20. M. Wu and T. Itoh, "Ultrafast Photonic to Microwave Transformer (PMT)," *LEOS Topical Meeting on Optical Microwave Interactions,* Paper W1.2, 1993.
21. A. Larsson et al., *J. Quantum Electron.*, vol. 24, 1988, p. 787.
22. D. L. Crawford, R. Nagarajan, and J. E. Bowers, "Comparison of Bulk and Quantum Wire Photodetectors," *Appl. Phys. Lett.*, vol. 58, no. 15, April 1991, pp. 1629–1631.
23. D. Kuhl, F. Hieronymi, E. H. Bottcher, and D. Bimberg, "High-Speed Metal-Semiconductor-Metal Photodetectors on InP: Fe," *IEEE Photon. Tech. Lett.,* vol. 2, no. 8, August 1990, p. 574.
24. Y. G. Wey, K. S. Giboney, J. E. Bowers, M. J. W. Rodwell, P. Silvestre, P. Thiagarajan, and G. Y. Robinson, "110 GHz GaInAs/InP *p-i-n* Photodiodes with Integrated Bias Tees and Matched Resistors," *IEEE Photonic Tech. Lett.,* August 1993.
25. D. M. Braun, "Design of Single Layer Antireflection Coatings for InP/InGaAs/InP Photodetectors for the 1200–1600 nm Wavelength Range," *Appl. Opt.*, vol. 27, 1988, pp. 2006–2011.
26. G. Lucovsky, R. F. Schwarz, and R. B. Emmons, "Transit-Time Considerations in *p-i-n* Diodes," *J. Appl. Phys.,* vol. 35, no. 3, March 1961.
27. J. E. Bowers and C. A. Burrus, "High Speed Zero Bias Waveguide Photodetectors," *Electron. Lett.*, vol. 22, 1986, p. 905.
28. A. Alping, R. Tell, and S. T. Eng, "Photodetection Properties of Semiconductor Laser Diode Detectors," *J. Lightwave Tech.,* vol. LT-4, 1986, pp. 1662–1668.
29. A. Alping, "Waveguide *p-i-n* Photodetectors: Theoretical Analysis and Design Criteria," *IEEE Proceedings,* vol. 136, part J, no. 3, June 1989.
30. S. Y. Wang and D. Bloom, "100 GHz Bandwidth Planar GaAs Schottky Photodiode," *Electron. Lett.,* vol. 19, no. 14, 7 July, 1983, p. 554.
31. D. G. Parker and P. G. Say, "Indium Tin Oxide/GaAs Photodiodes for Millimetric-Wave Applications," *Electron. Lett.,* vol. 22, no. 23, 6 Nov. 1986, p. 1266.
32. H. Kamiyama, Y. Kobayashi, T. Nagatsuma, and T. Kamiya, "Very Short Electrical Pulse Generation by a Composite Planar GaAs Photodetectors," *Jpn. J. Appl. Phys.,* vol. 29, Sept. 1990, p. 1717.
33. S. M. Sze, *Physics of Semiconductor Devices,* 1981, pp. 255–263.
34. M. Missous and E. H. Rhoderick, "On the Richardson Constant for Aluminum/Gallium Arsenide Schottky Diodes," *J. Appl. Phys.,* vol. 69, no. 10, 15 May 1991, p. 7142.
35. M. Kamegawa, K. Giboney, J. Karin, S. Allen, M. Case, R. Yu, M. J. W. Rodwell, and J. E. Bowers, "Picosecond GaAs Monolithic Optoelectronic Sampling Circuit," *Photonics Technology Lett.,* vol. 3, no. 6, June 1991, pp. 567–569.
36. E. Ozbay, K. D. Li, and D. M. Bloom, "2.0 psec GaAs Monolithic Photodetector," *IEEE Photon. Tech. Lett.,* vol. 3, no. 6, June 1991, p. 570.
37. N. Emeis, H. Schumacher, and H. Beneking, "High-Speed GaInAs Schottky Photodetector," *Electron. Lett.,* vol. 21, no. 5, 28 Feb. 1985, p. 181.
38. L. Yang, A. S. Sudbo, R. A. Logan, T. Tanbun-Ek, and W. T. Tsang, "High Performance Fe:InP/GaAs Metal/Semiconductor/Metal Photodetectors Grown by Metalorganic Vapor Phase Epitaxy," *IEEE Photon. Tech. Lett.,* vol. 2, no. 1, January 1990, p. 56.
39. T. Mikawa, H. Kuwatsuka, Y. Kito, T. Kumai, M. Makiuchi, S. Yamazaki, O. Wada, and T. Shirai, "Flip-Chip InGaAs Avalanche Photodiode with Ultra Low Capacitance and Large Gain-Bandwidth Product," *Tech. Digest,* ThO_2, OFC 1991, p. 186.
40. H. Kuwatsuka, T. Mikawa, S. Miura, N. Yasuoka, T. Tanahashi, and O. Wada, "An AlxGa1-xSb Avalanche Photodiode with Gain Bandwidth Product of 90 GHz," *Photon. Tech. Lett.,* vol. 2, no. 1, Jan 1990, p. 54.

41. F. Capusso, H. M. Cox, A. L. Hutchinson, N. A. Olsson, and S. G. Hummel, "Pseudo-Quaternary GaInAsP Semiconductors: A New $In_{0.53}Ga_{0.47}As$/InP Graded Gap Superlattice and Its Applications to Avalanche Photodiodes," *Appl. Phys. Lett.*, vol. 45, no. 11, 1 December 1984, pp. 1193–1195.
42. L. E. Tarof, "Planar InP/InGaAs Avalanche Photodiodes with a Gain-Bandwidth Product Exceeding 100 GHz," *Tech. Digest,* ThO3, OFC 1991, p. 187.
43. K. Taguchi, T. Torikai, Y. Sugimoto, K. Makito, and H. Ishihara, "Planar-Structure InP/InAsAsP/InGaAs Avalanche Photodiodes with Preferential Lateral Extended Guard Ring for 1.0–1.6 μm Wavelength Optical Communication Use," *J. Lightwave Tech.,* vol. 6, no. 11, Nov. 1988, p. 1643.
44. T. Shiba, E. Ishimura, K. Takahashi, H. Namizaki, and W. Susaki, "New Approach to the Frequency Response Analysis of an InGaAs Avalanche Photodiode," *J. Lightwave Tech.,* vol. 6, no. 10, Oct. 1988, p. 1502.
45. K. Berchtold, O. Krumpholz, and J. Suri, "Avalanche Photodiodes with a Gain-Bandwidth Product of More Than 200 GHz," *Appl. Phys. Lett.,* vol. 26, no. 10, 15 May 1975, p. 585.
46. T. Kagawa, H. Asai, and Y. Kawamura, "An InGaAs/InAlAs Superlattice Avalanche Photodiode with a Gain Bandwidth Product of 90 GHz," *IEEE Photon. Tech. Lett.* vol. 3, no. 9, September 91, pp. 815–817.
47. H. Imai and T. Kaneda, "High-Speed Distributed Feedback Lasers and InGaAs Avalanche Photodiodes," *J. Lightwave Tech.,* vol. 6, no. 11, Nov. 1988, p. 1643.
48. H. C. Hsieh and W. Sargeant, "Avalanche Buildup Time of an InP/InGaAsP/InGaAs APD at High Gain," *J. Quantum Electron.,* vol. 25, no. 9, Sept. 1989, p. 2027.
49. F. Osaka, T. Mikawa, and T. Kaneda, "Impact Ionization of Electrons and Holes in (100)-Oriented Ga1—xInxAsyP1-y," *IEEE J. Quantum Electron.,* vol. QE-21, no. 9, September 1985, pp. 1326–1338.
50. C. A. Lee, R. A. Logan, R. L. Batdorf, J. J. Kleimack, and W. Wiegmann, "Ionization Rates of Holes and Electrons in Silicon," *Phys. Rev.*, vol. 134, 1964, pp. A761–A773.
51. R. B. Emmons, "Avalanche-Photodiode Frequency Response," *J. Appl. Phys.,* vol. 38, no. 9, August 1967, p. 3705.
52. S. L. Miller, "Avalanche Breakdown in Germanium," *Phys. Rev.,* vol. 99, Aug. 1955, pp. 1234–1241.
53. R. J. McIntyre, "Multiplication Noise in Uniform Avalanche Junctions," *IEEE Trans. Electron. Devices,* vol. ED-13, Jan. 1966, pp. 164–168.
54. B. L. Kasper and J. C. Campell, "Multigigabit-per-Second Avalanche Photodiode Lightwave Receivers," *J. Lightwave Tech.,* vol. LT-5, no. 10, October 1987, p. 1351.
55. M. Brain and T. P. Lee, "Optical Receiver for Lightwave Communication Systems," *J. Lightwave Tech.,* vol. LT-3, no. 6, December 1985, p. 1281.
56. T. V. Muoi, "Receiver Design for High-Speed Optical-Fiber Systems," *J. Lightwave Tech.,* vol. LT-2, no. 3, June 1984, p. 243.
57. J. A. Caldmains and G. Mourou, "Subpicosecond Electrooptic Sampling: Principles and Applications," *IEEE J. Quantum Electron.,* vol. QE-22, 1986, pp. 69–78.
58. D. R. Grischkowsky, M. B. Ketchen, C.-C. Chi, I. N. Duling, III, N. J. Halas, J-M Halbout, and P. G. May, "Capacitance Free Generation and Detection of Subpicosecond Electrical Pulses on Coplanar Transmission Lines," *IEEE J. Quantum Electron.,* vol. 24, no. 2, February 1988, pp. 221–225.
59. W. C. Nunnally and R. B. Hammond, "Optoelectronic Switch for Pulsed Powers," *Picosecond Optoelectronic Devices*, C. H. Lee (ed.), Academic Press, Orlando, Fla., 1984, pp. 373–398.
60. F. W. Smith, H. Q. Le, V. Diadiuk, M. A. Hollis, A. R. Calawa, S. Gupta, M. Frankel, D. R. Dykaar, G. A. Mourou, and T. Y. Hsiang, "Picosecond GaAs-Based Photoconductive Optoelectronic Detectors," *Appl. Phys. Lett.*, vol. 54, no. 10, 6 March 1989, p. 890.
61. N. G. Paulter, A. J. Gibbs, and D. N. Sinha, "Fabrication of High-Speed GaAs Photoconductive Pulse Generators and Sampling Gates by Ion Implantation," *IEEE Trans. Electron Device,* vol. 35, no. 12, December 1988, pp. 2343–2348.
62. Y. Chen, S. Williamson, and T. Brock, "1.2 ps High Sensitivity Photodetector/Switch Based on Low-Temperature-Grown GaAs," Postdeadline papers, CPDP 10/591, CLEO 1991.